Electrochemical aptasensor of cellular prion protein based on modified polypyrrole with redox dendrimers

ARTICLE *in* BIOSENSORS & BIOELECTRONICS · DECEMBER 2013

Impact Factor: 6.41 · DOI: 10.1016/j.bios.2013.12.051 · Source: PubMed

Biosensors and Bioelectronics 56 (2014) 104–111

Contents lists available at ScienceDirect

Biosensors and Bioelectronics

journal homepage: www.elsevier.com/locate/bios

Electrochemical aptasensor of cellular prion protein based on modified polypyrrole with redox dendrimers

A. Miodek [a], G. Castillo [b], T. Hianik [b], H. Korri-Youssoufi [a,*]

[a] CNRS UMR-8182, Institut de Chimie Moléculaire et de Matériaux d'Orsay, Equipe de Chimie Bioorganique et Bioinorganique, Univ Paris-Sud, Bâtiment 420, 91405 Orsay, France

[b] Faculty of Mathematics, Physics and Informatics, Comenius University, Mlynska dolina F1, 84248 Bratislava, Slovakia

ARTICLE INFO

Article history:
Received 8 October 2013
Received in revised form
6 December 2013
Accepted 22 December 2013
Available online 31 December 2013

Keywords:
Biosensor
Polypyrrole
Aptamer
Dendrimers
Cellular prions
Electrochemical

ABSTRACT

This work consists of the development of an electrochemical aptasensor based on polyprrole modified with redox dendrimers, able to detect human cellular prions PrP^C with high sensitivity. The gold surface was modified by conductive polypyrrole film coupled to polyamidoamine dendrimers of fourth generation (PAMAM G4) and ferrocenyl group as redox marker. The aptamers were immobilized on the surface via biotin/streptavidin chemistry. Electrochemical signal was detected by ferrocenyl group incorporated between dendrimers and aptamers layers. We demonstrated that the interaction between aptamer and prion protein led to variation in electrochemical signal of the ferrocenyl group. The kinetics parameters (diffusion coefficient D and heterogeneous constant transfer k_{et}) calculated from electrochemical signals demonstrate that the variation in redox signal results from the lower diffusion process of ions during redox reaction after prion interaction due to bulk effect of larger protein. The association of redox dendrimers with conducting polypyrrole leads to high sensitivity of PrP^C determination with detection limit of 0.8 pM, which is three orders of magnitude lower, compared to flat ferrocene-functionalized polypyrrole. Detection of PrP^C in spiked blood plasma has been achieved and demonstrated a recovery up to 90%.

1. Introduction

Prion proteins are responsible for the transmissible spongiform encephalopathies (TSEs), which is a group of fatal neurodegenerative diseases. This includes Creutzfeldt–Jakob disease in human and spongiform encephalopathy in animals (Collinge, 2001). The diseases are highly contagious with possible transmission from animals to humans. It is assumed, that these diseases are caused by transformation of cellular prions (PrP^C) into their infectious isoform PrP^{Sc} (Masters et al., 1981; Prusiner, 1991). PrP^{Sc} differs from PrP^C in high content of β sheets, in resistance to protease digestion and in tendency to form large aggregates that cause formation of amyloid plaques in brain of mammals (Pan et al., 1993; Prusiner et al., 1998). Detection of prion using immunological techniques (Western blot and ELISA) is one of the most accurate method (Nunnally, 2002; Ingrosso et al., 2002). However, these methods are based on rather expensive antibody–enzyme conjugates, are time consuming and require qualified staff. Therefore the development of inexpensive, label-free rapid, sensitive and easy to use method for the detection of PrP^{Sc} is crucial for early diagnostics of prion diseases. Especially useful would be point-of-care assay that can be used even by physicians, outside of specialized clinical laboratories (Fournier-Wirth et al., 2010). So far, mostly the immunodiagnostic procedure (Safar et al., 2005) and post-mortem histopathological identification of brain tissues were applied (Kawatake et al., 2006; Kuczius et al., 2007). However, in contrast with cerebrospinal fluid, the concentration of PrP^{Sc} in the blood is down to pM (Panigaj et al., 2011), which makes the measurement difficult to achieve.

Biosensor technology, which is growing substantially in recent years, can help to overcome existing difficulties. The development of biosensors requires the achievement of an efficient interface between the biomolecules and the electronic transducers. Conducting polymers (CPs) are widely used as a transducer for biological interactions. In fact, CPs are polyconjugated polymers with an electronic structure giving them intrinsic characteristics such as electrical conductivity which can be controlled by a doping/de-doping process, low ionization potential, high electron affinity and optical properties. The electronic structure of conducting polymers is very sensitive to any modification of the backbone conjugation and conformation related to the biological interaction (Tlili et al., 2005). Thus, the success of CPs as a transducer relies on their combined versatility in providing a suitable interface for grafting bioreceptors onto micron-sized surfaces (Livache et al., 1998; Grosjean et al., 2005) and in their ability to

* Corresponding author. Tel.: +33 1 69157440; fax: +33 1 69157281.
E-mail address: hafsa.korri-youssoufi@u-psud.fr (H. Korri-Youssoufi).

0956-5663/$ - see front matter © 2013 Elsevier B.V. All rights reserved.
http://dx.doi.org/10.1016/j.bios.2013.12.051

monitor the biological recognition transfer produced by probe/target interactions to a measured signal which is related to their optical (Ho et al., 2005) or electrical properties (Korri-Youssoufi et al., 1997). The most commonly used CP in sensing applications is polypyrrole (PPy) owing to its biocompatibility, high hydrophilic character and high stability in water (Ramanavičius et al., 2006). The poly(amidoamine) dendrimers of fourth generation (PAMAM G4) have been successfully applied in the fabrication of biosensors (Zhu et al., 2010). PAMAM G4 has a globular structure with diameter of about 4.5 nm and possesses 64 primary amine groups on the surface (Tsukruk et al., 1997). The amino groups with high density in PAMAM are easily functionalized by other substances that greatly extend their applications in biosensors (Shi et al., 2008). PAMAM dendrimer could be directly substituted by pyrrole monomer and then electropolymerized on surface (Şenel and Nergiz, 2012; Şenel and Çevik, 2012) or covalently attached to modified polypyrrole through amide link.

The aim of this work lies in the development of an electrochemical biosensor for real time detection of cellular prion proteins (PrP^C). A biosensor is based on covalent attachment of PAMAM G4 to the functionalized polypyrrole layer, electropolymerized on the surface of a gold electrode. High number of amine groups on the surface of PAMAM has been exploited for covalent attachment of ferrocenyl group (Fc) as redox markers. Aptamers have been selected due to their sensitivity to prion proteins (Bibby et al., 2008) and the sequence used selected from Takemura et al. (2006) was extended by a 15-mer thymine spacer in order to provide more flexibility of the aptamers for the anchoring to the layer.

2. Materials and methods

2.1. Reagents

The human prion protein, PrP^C (103-231) molecular weight 15.1 kDa was purified in INRA Jouy-en-Josas in France by Dr. Human Rezaei and Jasmina Vidic. The aptamers specific for PrP^C (103-231) with dT_{15} spacer and biotinylated on 3′ phosphoryl terminus (5′-CGG TGG GGC AAT TTC TCC TAC TGT dT_{15}-3′-Biotin) (Biopri) were provided by Thermo Fisher Scientific (Germany) and dissolved in TE buffer consisting of 10 mM tris(hydroxymethyl) aminomethane (Tris) and 1 mM ethylene di-amine tetra-acetic acid (EDTA) at pH 7.6 in double distilled water.

Pyrrole (Py) was purchased from Sigma-Aldrich and distilled in argon before use. The 3-(N-hydroxyphthalimidyl ester) pyrrole PyNHP, 1-(phthalimidylbutanoate)-1′-(N-(3-butylpyrrole)butanamide) ferrocene PyFcNHP and 1,1′-(phtalimidebutanoate) ferrocene $Fc(NHP)_2$ were synthetized according to the methods previously described (Korri-Youssoufi and Yassar, 2001; Korri-Youssoufi and Makrouf, 2001). The poly(amidoamine) dendrimers (PAMAM) of fourth generation (G4) were purchased from Sigma-Aldrich and filtered by 0.22 μM membrane filters before use. Biotin hydrazide and streptavidin were also purchased from Sigma-Aldrich. All analyses were performed in phosphate buffer saline (PBS) pH 7.4 containing 10 mM Na_2HPO_4, 1.8 mM KH_2PO_4, 2.7 mM KCl and 137 mM NaCl, filtered by 0.22 μm membranes and stored at 4 °C until use. Non-specific interactions were studied using Bovine Serum Albumin (BSA) (Sigma-Aldrich).

2.2. Instrumentation

Electrochemical polymerization and characterization were performed using a potentiostat–galvanostat Autolab PGSTAT 12 controlled by GPES software. The three-electrode cell was purchased from BASi and consists of a platinum mesh as a counter-electrode, gold disc (surface 2.01×10^{-2} cm^2) as a working electrode and Ag/AgCl as a reference electrode. After polymerization and each step of construction of the biosensor, the modified surface was analyzed in 10 mM PBS buffer pH 7.4 by the CV (cyclic voltammetry) method. CV was performed by cycling the potential from −0.4 to 0.4 with the scan rate of 100 mV s^{-1}. DPV (differential pulse voltammetry) was performed in the range of potential from −0.6 to 0.4 with conditioning time of 120 s and modulation amplitude of 50 mV.

Electrochemical impedance measurements (*EIS*) were carried out within 10 mM PBS buffer pH 7.4. All impedances were obtained at 0.15 V vs. Ag/AgCl at DC potential of 10 mV in a frequency range from 100 kHz to 0.1 Hz.

Chronoamperometric measurements were performed in PBS with 5 mM/5 mM $[Fe(CN)_6]^{4-}/[Fe(CN)_6]^{3-}$ at the potential of 0.2 V. The current was measured for 90 s.

Scanning Electron Microscopy (*SEM*) images were acquired using a ZEISS SUPRA™ 55VP GEMINI®. The copolymer film and the different steps of construction of the biosensor, for SEM analysis, were prepared by electropolymerization on the plate gold surface according to the method described in the Section 2.3.

2.3. Electropolymerization of copolymers PPy-PyNHP and PPy-PyFCNHP

The copolymer film consisting of two monomers, pyrrole (Py) and pyrrole functionalized by an active ester (PyNHP), was grown on gold surface immersed in acetonitrile containing 0.5 M $LiClO_4$ by cycling the potential from −0.4 to 1.2 V vs. Ag/AgCl at the scan rate of 100 mV s^{-1}. The reaction was stopped when a current intensity corresponding to redox signal of polypyrrole reached 13 μA. During the electropolymerization the working and counter-electrodes were separated in a small volume cell (BASi) containing the solution of two monomers. The ratio of Py to modified pyrroles PyNHP or PyFcNHP used during reaction was 8:2 mM according to the optimal conditions described previously (Lê et al., 2010a, 2010b). The copolymer film of PPy-PyFcNHP was grown under the same conditions by cycling the potential from −0.4 to 0.95 V vs. Ag/AgCl and the reaction was stopped when a current intensity corresponding to ferrocene reached 30 μA to obtain the same thickness as obtained previously. After polymerization, the copolymer films were analyzed in PBS buffer by the CV method (see Section 2.2 for conditions).

2.4. Construction of the biosensor

Covalent bonding of dendrimers PAMAM to the modified polypyrrole PPy-PAMAM was performed by immersing the modified electrode in 70 μM of aqueous solution of PAMAM for 2 h at room temperature followed by washing the electrode with distilled water and PBS buffer for removing the non-linked residues. Then, ferrocene modified by two phtalymidyl $Fc(NHP)_2$ groups was associated with the surface. Reaction was performed by immersing the electrode in 1 mM solution of ferrocene for 1 h at room temperature. Non-bonded residues were washed by acetonitrile and double distilled water. Subsequently, the electrode was dipped in 40 μl of solution of 2 mg mL^{-1} biotin hydrazide in PBS buffer for 45 min at room temperature. Then non-bonded residues were removed by washing the electrode with distilled water and PBS buffer. Afterwards, the electrode was incubated for 45 min in solution of 100 μg $ml^{-1}$of streptavidin in PBS at room temperature followed by washing the electrode with distilled water and PBS buffer. Aptamer attachment on the surface was obtained by dipping the electrode in 2 μM biotinylated aptamers solution in PBS buffer for 45 min at room temperature. Then the biosensor was carefully washed with distilled water and PBS buffer and stored in PBS buffer at 4 °C during 1 night. After each step of construction of the aptasensor, the surface modifications were controlled by the CV method (see Section 2.2 for conditions).

2.5. Prion detection

The human prion protein PrP^C (103-231) was detected in the range of concentrations from 1 pM to 1 μM. The incubation was performed by immersing the electrode with a sensing layer in various ranges of concentrations of prion protein (1, 10, 100 pM, 1, 10, 100 nM, and 1, 10 μM), subsequently from lower to higher concentration, for 40 min at room temperature. Then the electrode, between each measurement and incubation, was washed by distilled water and PBS. Six individually prepared biosensors were tested. The reproducibility of the sensor preparation was up to 3%.

3. Results and discussion

3.1. Modifications of copolymer PPy-PyNHP with redox PAMAM G4 dendrimers

Electropolymerization of two monomers Py and PyNHP was performed by scanning potential from −0.4 to 1.2 V (vs. Ag/AgCl) in acetonitrile containing 0.5 M $LiClO_4$ under the same conditions as described previously (Miodek et al., 2013a). The optimal ratio of monomers for biosensor construction was determined in our previous work (Lê et al., 2010a) to 8:2 mM of Py:PyNHP as 8:2. This leads to obtaining deposit film on gold surface with 10 nm thickness as demonstrated previously using SPR analysis (Miodek et al., 2013a). Modification of Py by active ester NHP allows binding dendrimers through their amine groups by amido-link (see Fig. 1). The morphology of the two, copolymers PPy-PAMAM before and after dendrimer attachment, was studied by SEM. Fig. 2A presents SEM images of copolymer film PPy-PyNHP. The morphology of the copolymer layer shows a rough and compact morphology with a typically granular raspberry structure of polypyrrole as generally observed (Chen et al., 2006). However, the PPy-PAMAM film exhibits a structure with small aggregates deposited on the surface (Fig. 2B). The surface morphology change of PPy-PAMAM is ascribable to the existence of PAMAM nanoparticles uniformly linked to the polymer layer.

Association of ferrocene as a redox marker with the PPy–PAMAM layer was performed chemically by covalent link of modified ferrocene with two carboxylic groups—COOH activated by phtalimydyl (NHP) (Korri-Youssoufi and Makrouf, 2001). The ferrocenyl groups were covalently attached to the PAMAM dendrimers to assemble the PPy–PAMAM–Fc layer (see Fig. 1). The

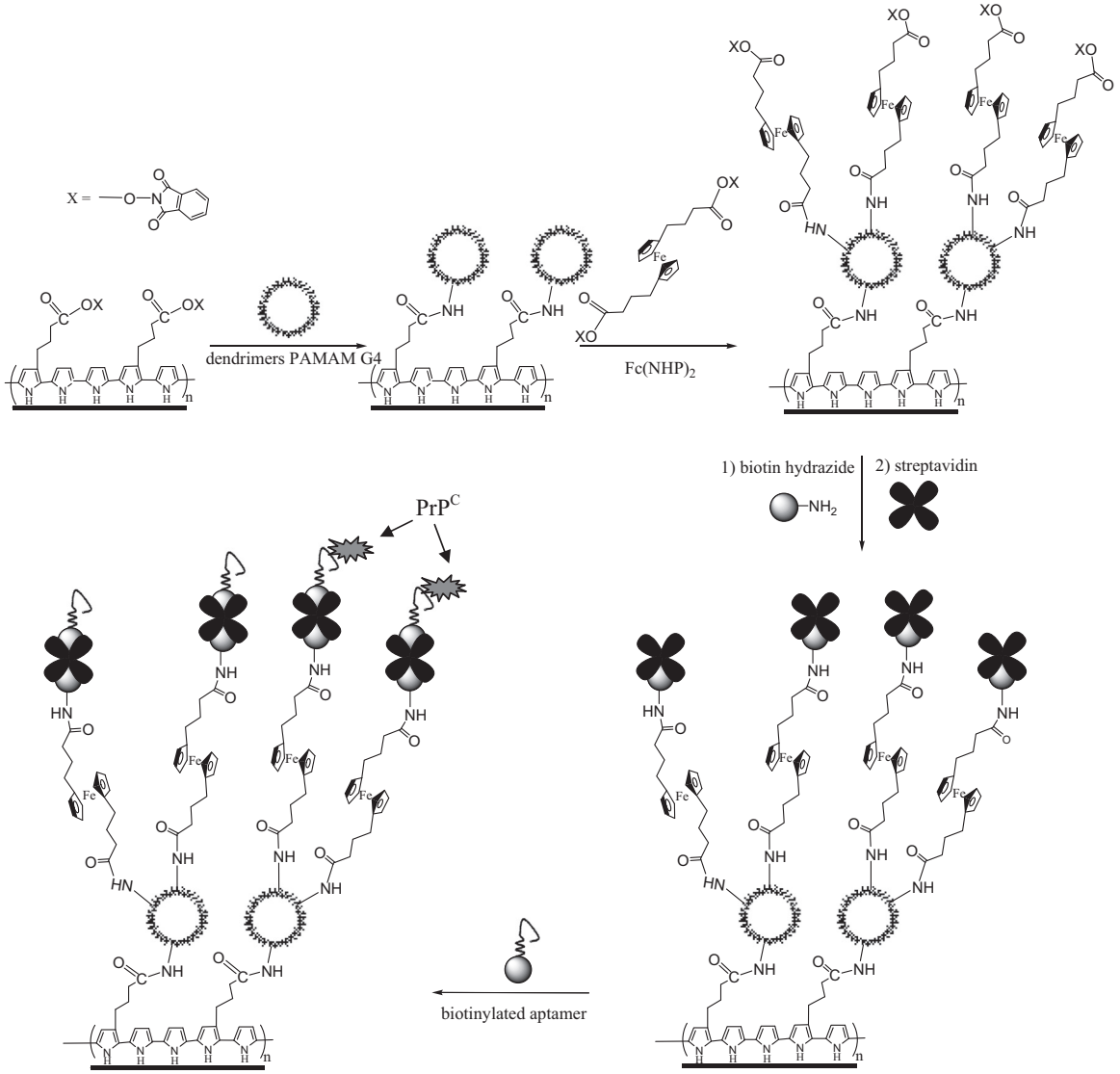

Fig. 1. Schematic representation of a biosensor showing various steps of biolayer formation on gold surface, PPy electropolymerization, PAMAM covalent attachment, ferrocene covalent attachment, biotin covalent attachment, streptavidin interaction and biotinylated aptamer interaction.

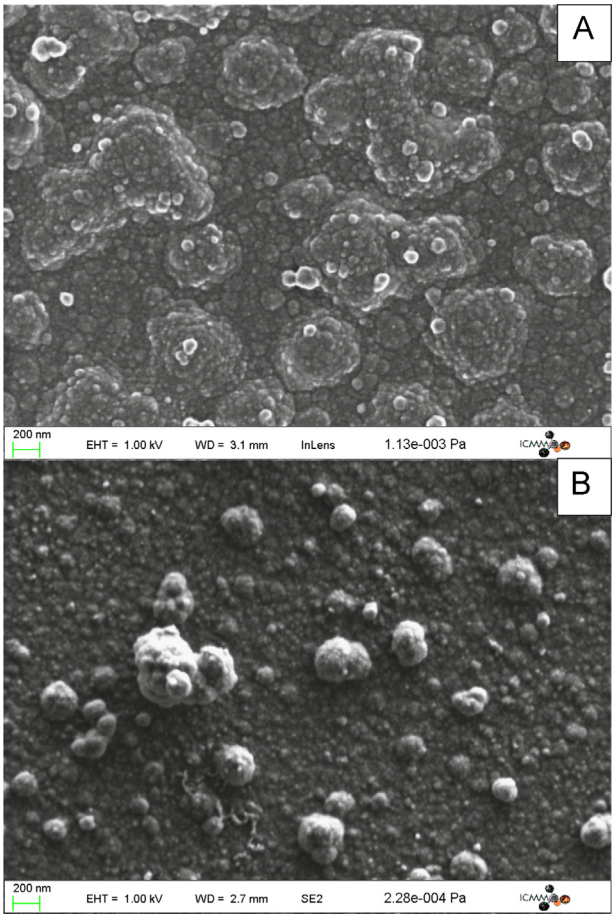

Fig. 2. SEM images of gold surface covered by (A) PPy-PyNHP and (B) PPy–PAMAM.

electrochemical properties of formed biolayer (PPy–PAMAM–Fc) were studied by cyclic voltammetry (CV) and by electrochemical impedance spectroscopy (EIS). Fig. 3A shows the CV curves before and after bonding of ferrocene to the surface modified with PPy–PAMAM. Covalent attachment of ferrocene to PAMAM leads to the appearance of characteristic reversible redox signal of ferrocene with oxidation and reduction peaks at 0.11 V and 0.05 V (vs. Ag/AgCl), respectively. The variation of the redox signal with the scan rate was analyzed by variation of potential from 0.005 V s^{-1} to 1 V s^{-1}. The CV curves show an increase in current with scan rate (Fig. 3B). The increase in the anodic and cathodic currents with the scan rate (Fig. 3B, upper inset) was linear from 0.2 V s^{-1} to 1 V s^{-1}. This demonstrates the surface-controlled process of charge transfer (Bard and Faulkner, 2001). At relatively low scan rate as 5 mV s^{-1} there was no difference between potentials of anodic and cathodic peaks, suggesting the reversible redox process. At high scan rate of 1 V s^{-1}, the anodic and cathodic peaks were still well defined and the difference between potentials of anodic peaks at low and high scan rates (ΔE_p) was less than 0.2 V, indicating a significant rate of electron transfer.

The charge exchanged during the redox process allows calculation of the surface coverage of redox dendrimers following the equation:

$$\Gamma = \frac{Q}{nFA} \quad (1)$$

where Q is the charge under the cathodic or anodic waves, n is number of electrons involved in the redox process, F is the Faraday constant, and A is the area of the electrode. We estimated that the average coverage of the surface by ferrocene was 3.00 ± 0.04 nmol cm^{-2}. Optimum coverage of a redox marker is needed to obtain high variation during detection step. The optimum is reached when each immobilized ferrocene could attach biomolecules and detect the target. This average coverage is low compared to that obtained for polypyrrole formed with modified monomers bearing ferrocene which is 25.7 ± 0.4 nmol cm^{-2} (Lê et al., 2010b). However, it is higher than the value obtained for a monolayer of ferrocene (0.12 pmol cm^{-2}) (Liu et al., 2005). Thus, this approach allows immobilization of high coverage of the redox marker with high dispersion taking large size of biomolecules into account, thanks to three dimensional architectures of the dendrimers.

Impedance measurements were performed to analyze the electrical properties of such layers. They have been performed in PBS solution. The EIS data were fitted according to the Randles equivalent circuit model, where R_s is the electrolyte resistance and R_{ct} is the electron transfer resistance; double layer capacitance was replaced by constant phase element CPE_1 and the Warburg impedance Z_w was replaced by another constant phase element CPE_2. CPE behavior is obtained when the distribution of time constant is not linear on the entire surface. The impedance of CPE could be written as $Z_{CPE}=1/Q(j\omega)^n$, where Q and n are independent of the frequency, ω is the radial frequency and n is a dimensional parameter with the value $-1<n<1$; for $n=1$ a pure capacitance is obtained; if $n=0.5$ Warburg impedance is obtained, and when $0<n<1$ the impedance is CPE. The analytical treatment of impedance data allows the demonstration of CPE behavior. This could be obtained by plotting the logarithm of real part of impedance ($\log Z'$) vs. logarithm of frequency ($\log f$); the value of n determines the CPE behavior. In this study, n was around −0.6 to −0.7 suggesting that CPE could replace the capacitance. The EIS data were satisfactory fitted by the modified equivalent circuit model shown in inset of Fig. 3D as demonstrated by an error value. The fit also allowed determining electrical parameters for each layer formation. The capacitance was directly related to the thickness of the layer. From the capacitance value obtained with various layers PPy–PyNHP and PPy–PAMAM the thickness of dendrimer's layer could be estimated

$$C = \frac{A\varepsilon_0\varepsilon_1}{d} \quad (2)$$

where ε_0 is the vacuum dielectric constant, ε_1 is the double layer dielectric constant, A is the surface area and d is the thickness of the layer. The thickness of the layer PPy–PAMAM–Fc could be calculated from the variation of capacitance value obtained from the film PPy–PyNHP and PPy–PAMAM–Fc. The value was calculated to be 4.05 ± 0.06 nm which corresponded to the size of dendrimer PAMAM G4 and confirmed the immobilization of monolayer of PAMAM, thanks to covalent attachment.

3.2. Formation of a biolayer and cellular prion detection

The first step of biolayer construction was the covalent attachment of biotin hydrazide to the ferrocene, followed by immobilization of streptavidin, thanks to surface modified by streptavidin for immobilization of biotinylated aptamer to the surface. The construction of the biosensor was monitored by CV and EIS methods in PBS buffer pH 7.4. Fig. 3C shows the voltammograms performed after each step of biosensor construction. The intensity of the redox signal corresponding to ferrocene decreases. These phenomena could be related to the low electron transfer or to slow diffusion of electrolyte to surface during the redox process due to the attachment of the large molecules to the surface and was observed previously (Lê et al., 2010a; Chebil et al., 2010).

Detection of human prion protein was performed using CV and differential pulse voltammetry (DPV) methods. The biosensor was incubated with successive addition of various prion concentrations from 1 pM to 10 μM. Fig. 4A shows the decrease in current

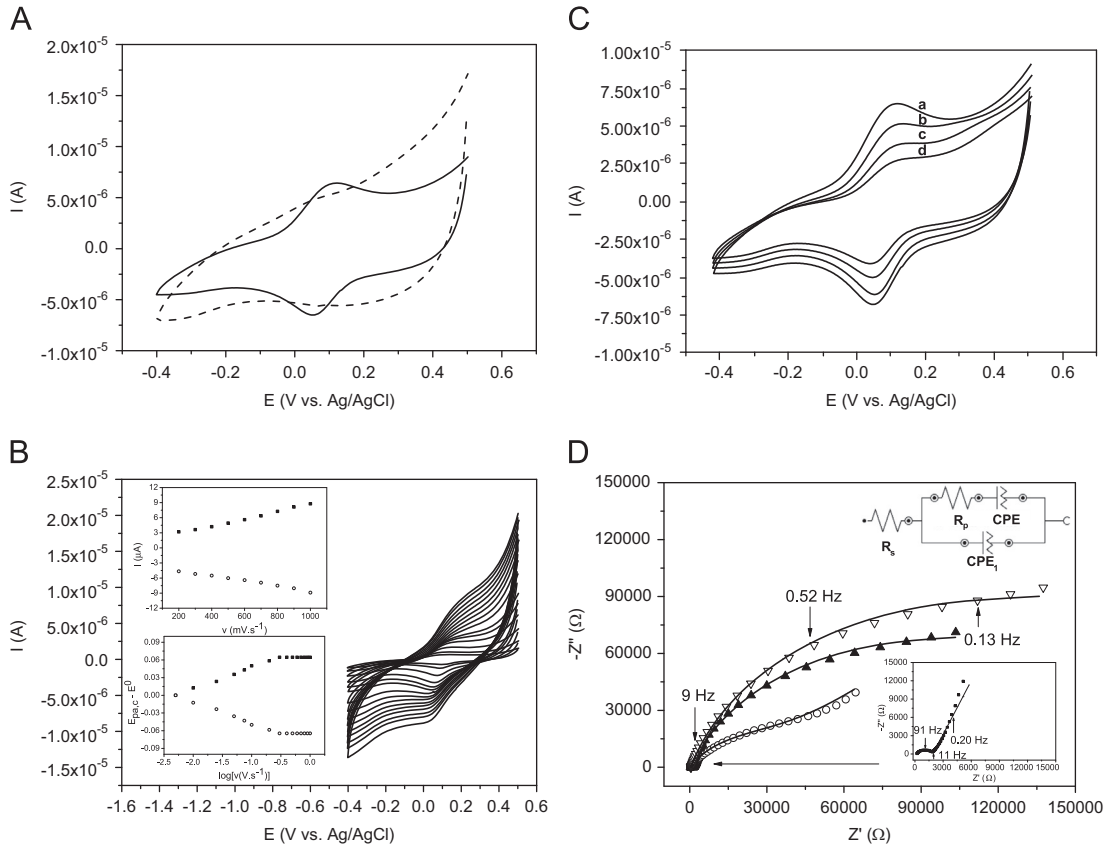

Fig. 3. (A) Cyclic voltammogram of electrochemical signal of ferrocenyl group (Fc) linked to polypyrrole modified with PAMAM G4 dendrimers PPy–PAMAM–Fc (solid line) and compared to PPy–PAMAM (dotted line) before modification by Fc; (B) CV at various scans of a gold electrode covered by PPy–PAMAM–Fc in the range 0.005–1 V s^{-1}. The upper inset shows the variation of anodic and cathodic current peaks vs. scan rate and lower inset shows the variation of anodic ($E_{p,a}$–E^0) and cathodic potentials ($E_{p,c}$–E^0) vs. logarithm of scan rate; (C) CV data obtained after each step of biosensor formation: curve (a) PPy–PAMAM–Fc, curve (b) PPy–PAMAM–Fc–biotin, curve (c) PPy–PAMAM–Fc–biotin–streptavidin and curve (d) PPy–PAMAM–Fc–biotin–streptavidin–aptamer; (D) Nyquist plot obtained in PBS, pH 7.4 at various steps of biosensor formation: PPy–PAMAM–Fc (○), PPy–PAMAM–Fc–biotin–streptavidin–aptamer (▲), and PPy–PAMAM–Fc–biotin–streptavidin–aptamer obtained after incubation with 1 μM of PrP^C (▽). Inset—the Nyquist plot of the gold electrode covered by the PPy–PyNHP layer. The impedance measurements were obtained in frequency range from 0.1 Hz to 100 kHz at 0.15 V vs. Ag/AgCl by applying DC potential of 10 mV. The symbols are the experimental data and the solids are the fitted curves using the equivalent circuit shown in inset.

corresponding to redox signal of ferrocene after incubation with each prion concentration. The decrease in the current was also observed within the DPV method (Fig. 4B). This variation in current intensity can be explained by association of prion protein with the immobilized aptamers, which avoid the penetration of ions and decrease of the electron transfer. The same results were obtained with the immunosensor developed with polypyrrole layers (Lê et al., 2010a) or polypyrrole associated with a redox probe (Chebil et al., 2010; Lê et al., 2010b).

3.3. Kinetics characterization of electrochemical aptasensors

In order to analyze the origin of current variation after interaction of aptamer with prion, the electrochemical parameters of this layer were analyzed by means of kinetics of electronic transfer of the ferrocene; it is permeability of the layer to ions diffusion during the redox process. The rate of heterogeneous electron transfer (k_s) was determined following the Laviron model by measuring the variation of redox peak potential within scan rate (Fig. 3B). This can be obtained following the equation developed by Laviron (1979) with the Butter–Volmer model:

$$m = \left(\frac{RT}{F}\right)\frac{k_s}{nv} \tag{3}$$

$$k_s = m\left(\frac{F}{RT}\right)nv \tag{4}$$

The value m was determined by adjustment of the curve $\Delta E_p = f$ (m^{-1}) for coefficient of electron transfer $\alpha = 0.5$. The coefficient α was determined based on the variation in anodic potential ($E_{p,a}$–E^0) and cathodic potential ($E_{p,c}$–E^0) vs. logarithm of the scan rate (Fig. 3B, lower inset).

The k_s value obtained for PPy–PAMAM–Fc was calculated as $5.8 \pm 0.3\ s^{-1}$. The k_s value obtained is high compared to the layer where ferrocene was immobilized through monolayers surface where k_s has been reported to be $0.78\ s^{-1}$ (Liu et al., 2005) but still at the same order of magnitude for ferrocene immobilized through the monolayer of SWCNT ($9.5\ s^{-1}$) (Nkosi et al., 2010). This increase could be related to the effects of dendrimers where their chemical properties enhance the permeation of ions affecting the electron transfer. The k_s value measured for biolayer decreases to $3.3 \pm 0.2\ s^{-1}$ after the aptamer immobilization through the biotin streptavidin layer. Interaction of prions with a sensing layer leads to a small decrease in k_s value to $1.5 \pm 0.2\ s^{-1}$. This suggests that saturation of surface by prion proteins did not disturb the kinetic of electron transfer.

To confirm these parameters, the heterogeneous electron transfer through layers was determined by impedance data as the Butter–Volmer model overestimating the kinetic value. EIS measurement provides details in kinetics of charge transfer through the biolayer occurring at the electrodes. Fig. 3D shows

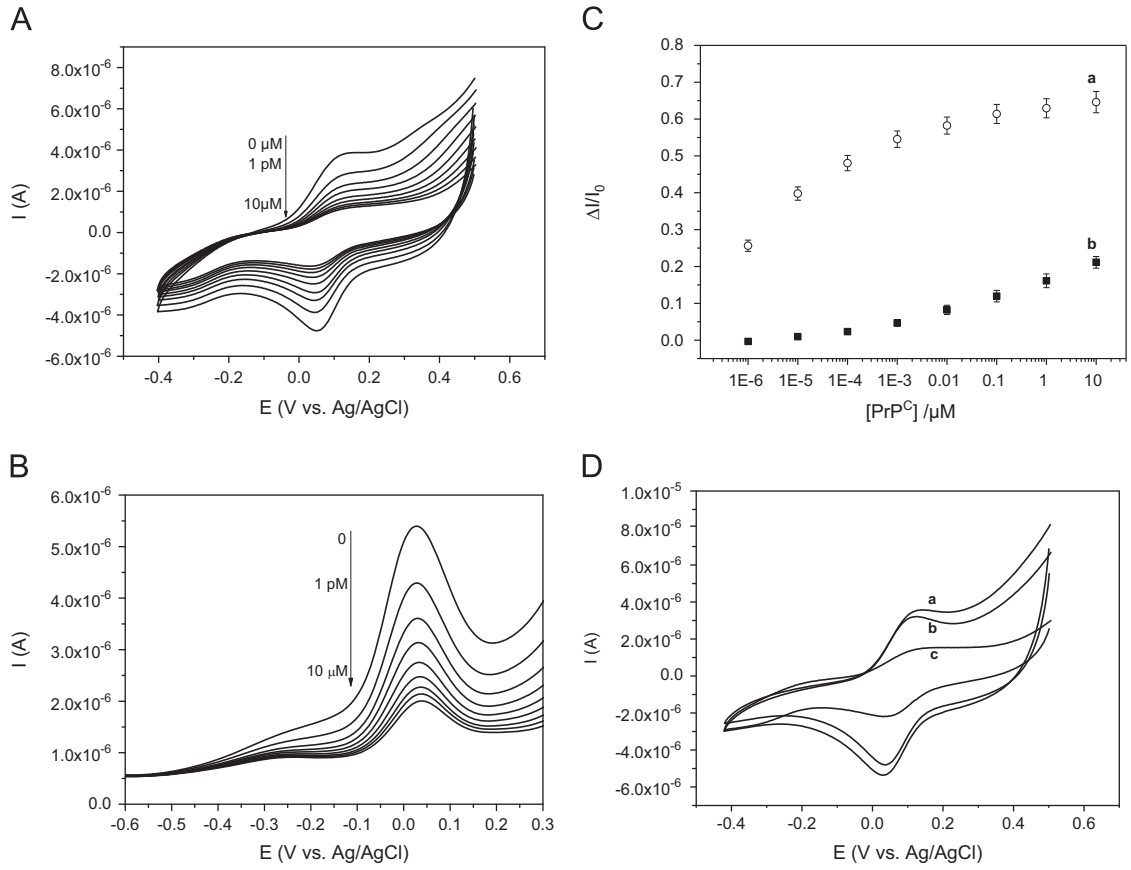

Fig. 4. (A) CV of biosensors after prion protein association with aptamer at various concentrations of PrP^C from 1 pM to 10 μM. CVs were recorded in PBS solution at pH 7.4 with scan rate of 100 mV s^{-1}. (B) DPV of biosensor at various concentrations (1 pM–10 μM) recorded in PBS solution with amplitude 50 mV s^{-1}. (C) The plot of the relative changes of the current peak vs. concentration of PrP^C (103-231) for the biosensors bearing PAMAM (a) and the layer without dendrimers PAMAM (b). $\Delta I=(I_0-I)$, where I_0 is the peak current prior addition of PrP^C and I after incubation of the sensor with certain concentration of PrP^C. (D) CV presents the results obtained for non-specific interactions compared to specific one. Curve (a) shows CV of biosensor after formation, curve (b) shows response of biosensor after incubation in solution of 1 μM BSA, and curve (c) shows response of biosensor after incubation in 1 μM of PrP^C.

the Nyquist plots obtained for the biolayer after ferrocene immobilization and then after biolayer formation. Immobilization of biolayer (biotin–streptavidin–aptamer) on the surface led to an increase in R_{ct} value. This effect could be related to the blocking of the biolayer to the permeation of redox species at the surface of electrode when such large molecules were immobilized on the surface.

The apparent heterogeneous electron transfer rate constant (k_{et}) can be calculated as follows:

$$k_{et} = \frac{1}{2R_{ct}\mathrm{CPE}_2} \tag{5}$$

where n is the number of electrons transferred in the redox process, F is Faraday constant, R is the gas constant, T is the temperature in Kelvin, A is the area of the electrode, and R_{ct} is the value of charge transfer resistance obtained from the fitted parameters of the Nyquist plot. Table 1 shows the k_s and k_{et} values obtained during all steps of biolayer formation and after prion interaction. The k_{et} values were lower in comparison with k_s; however the same behavior was obtained. k_{et} decreases after aptamer immobilization and remains constant after prion interaction, indicating that electrochemical reaction of redox species is slower when aptamers were immobilized on the surface. This result could be related to the negative charge of phosphate ions in aptamer sequence that prevents electron transfer of redox ferrocene. The same behavior has been obtained in the case of DNA biosensor (Tlili et al., 2005).

Another parameter that controls the redox process is the permeability of the layer to the ion diffusion. The permeability of the layer could be determined by measuring the diffusion coefficient of redox species from buffer solution to the electrode. This parameter could be obtained from the Cottrell law (Eq. (6)) by measuring the current vs. time during chronoamperometric reaction performed in solution containing 5 mM/5 mM $[Fe(CN)_6]^{4-}$/$[Fe(CN)_6]^{3-}$:

$$i(t) = nFAC^*\sqrt{\frac{D}{\pi t}} \tag{6}$$

where n is number of electrons involved in the redox process, F is the Faraday constant, A is the area of the electrode and C^* is the bulk concentration of Fe^{2+}/Fe^{3+}. Under diffusion control, $i=f(t^{-1/2})$ is linear and D value can be calculated based on the slope. The diffusion coefficient of $[Fe(CN)_6]^{4-}$/$[Fe(CN)_6]^{3-}$ ions on the Py–PAMAM–Fc layer was determined as $5.6 \pm 0.3 \times 10^{-6}$ cm^2 s^{-1}. It decreases to $2.2 \pm 0.2 \times 10^{-6}$ cm^2 s^{-1} after aptamers immobilization; however after prion interaction the coefficient of diffusion is lowered by one order of magnitude $0.20 \pm 0.04 \times 10^{-6}$ cm^2 s^{-1}. This result underlines that the ion permeation has an important effect on the electrochemical behavior of immobilized redox probe after protein immobilization.

3.4. Analytical performance of a biosensor

In order to study the aptasensor response, a calibration curve corresponding to the variation of the current at 0.11 V vs. prions

Table 1
Electrochemical parameters obtained from electrodes after various steps of biolayer modifications.

	α	k_s (s^{-1})	k_{et} (s^{-1})	D ($cm^2\ s^{-1}$)
PPy-PAMAM-Fc	0.50	5.8 ± 0.3	0.50 ± 0.03	$(5.6 \pm 0.3) \times 10^{-6}$
PPy-PAMAM-Fc-Aptamer	0.50	3.3 ± 0.2	0.05 ± 0.002	$(2.2 \pm 0.2) \times 10^{-6}$
PPy-PAMAM-Fc-Aptamer-PrP	0.50	1.5 ± 0.2	0.05 ± 0.002	$(0.2 \pm 0.04) \times 10^{-6}$

concentration in logarithmic scale was plotted (Fig. 4C, curve a) to show the dynamic range of detection. The prion protein was detected in the linear range from 1 pM to 1 nM (figure not shown) with limit of the detection (LOD) 0.8 pM (LOD has been calculated at signal (S) to noise (N) ratio S/N=3). The saturation of the biosensor was obtained at concentration of 10 nM. The reproducibility of the sensor was tested by six measurements made with six independent biosensors with a freshly prepared sensing layer. The bars represent standard deviation for six independents measurements that was calculated as 1.5–2.8% demonstrating high reproducibility of biosensors.

To show the influence of three-dimensional structure of PAMAM on the sensitivity of the biosensor, the prion protein was detected by a biosensor based on two monomers: pyrrole and pyrrole modified by ferrocenyl group and activated by NHP. This biosensor was described previously for DNA detection (Lê et al., 2010b). In this biosensor, biotin hydrazide was directly covalently bonded to the copolymer and then streptavidin and biotinylated aptamers were immobilized. The detection of protein was performed in the same concentration range from 1 pM to 10 μM, as used in the case of a ferrocenyl-modified pyrrole biosensor. During detection of prion the redox signal corresponding to ferrocene groups decreased. Using the variation of the current as a function of prion concentration, the calibration curve was plotted and compared to the biosensor formed with redox dendrimers (see Fig. 4C, curve b). The figure shows that this sensor shows higher sensitivity (LOD 0.8 pM) than that obtained without association of dendrimer (LOD 0.7 nM).

The non-specific interactions were studied using incubation of high concentration (1 μM) BSA. Fig. 4D (curve b) shows a small variation of the current ($8 \pm 2\%$) after incubation of biosensor in BSA solution which may be due to adsorption of some BSA on the surface of the biosensor as large concentration has been used. To compare the effect with prion protein the same concentration of 1 μM of prion PrP^C caused a variation in current of $63 \pm 2.5\%$ (Fig. 4D, curve c).

3.5. Detection in plasma

For validation of the practical application of the biosensor, 10-times diluted human blood plasma was spiked by PrP^C (103-231) in the same range of concentrations as used in PBS buffer (1 pM–10 μM). The dilution of plasma was performed in order to obtain comparable reference signal between measurements in plain buffer and those in human plasma. For non-diluted plasma samples the reference signal given by the biosensor was much higher than the signal of biosensor obtained in buffer, presumably due to the presence of various proteins in plasma. This higher signal in plasma would make the calculation of the biosensor recovery more complicated. Therefore the plasma was diluted and further filtrated through 0.22 um pore filters. Once prion was added, the biosensor was immersed into the spiked serum for 40 min at room temperature and then rinsed with PBS buffer. Subsequently the cyclic voltammograms were recorded. Six independent measurements were performed. First, to avoid non-specific interactions, the biosensor was incubated in the plasma sample which did not contained PrP^C. The response of the sensor measured after incubation in this plasma samples was used as a reference signal (I_0). Then the sensor response (I) was measured at certain PrP^C concentrations of spiked plasma, and the relative changes of the current $\Delta I/I_0$ have been calculated ($\Delta I = I_0 - I$). The results are presented in Table 2. It can be seen that the sensor response in spiked plasma agrees well with the response in PBS. The sensor demonstrated a recovery of a minimum of 90.98% corresponding to 1 μM PrP^C and a maximum of 101.55% corresponding to 1 pM PrP^C in PBS. The sensor recovery has been calculated as a ratio of the sensor response for spiked plasma to that obtained in buffer for identical prion concentrations. This ratio has been multiplied by 100 to obtain the recovery in %. Evidently, some fraction of plasma covering the free sites of the electrode especially at the lowest prion concentration as 1 pM lead to the sensor recovery values of 101.55%. The sensor recovery in all ranges of prion concentration reached 90.98–101.55% of detection in plasma which shows good agreement with detection obtained in PBS buffer. The recovery was better in comparison with recently reported biosensor based on PAMAM G4 and multiwalled carbon nanotubes, although the sensitivity of PrP^C detection in later case was comparable (LOD=0.5 pM) (Miodek et al., 2013b). In real application measurement, the incubation with plasma sample will be included in protocol preparation. This should be done by using various samples of both, healthy persons and commercial normal control plasma, which is generally collected from a minimum of 20 healthy donors.

Table 2
Detection of prion proteins in human plasma. Results represent mean ± SD (standard deviation) obtained from six independent experiments.

PrP added (μM)	PrP found (μM)	R.S.D. (%)	R.E. (%)	Recovery (%)
10^{-6}	1.02×10^{-6}	6.02	1.56	101.55
10^{-5}	9.76×10^{-6}	4.45	2.35	97.65
10^{-4}	9.73×10^{-5}	4.21	2.70	97.30
10^{-3}	9.64×10^{-4}	3.93	3.60	96.40
10^{-2}	9.43×10^{-3}	3.76	5.73	94.27
10^{-1}	9.39×10^{-2}	3.96	6.06	93.94
1	9.10×10^{-1}	3.74	9.02	90.98
10	9.23	4.13	7.69	92.30

R.S.D. (relative standard deviation)=standard deviation/mean × 100%; R.E. (relative error)=[(true value − measured value)/true value] × 100%; n=6.

4. Conclusions

Biolayer formed with conducting polypyrrole and PAMAM G4 dendrimers connected to redox marker ferrocene is demonstrated to be an efficient platform for development of electrochemical aptasensors in the case of detection of human cellular prion protein (PrP^C). We demonstrated that immobilization of optimum redox ferrocene through layer of PAMAM dendrimers on conducting surface of polypyrrole allowed high electron transfer rate. Prion detection was obtained through variation of redox signal of the immobilized redox marker and demonstrates high sensitivity to the formation of complex aptamer/prion on the surface where detection limit of 0.8 pM was obtained. The aptasensor was

validated by detection of prion protein in spiked human blood plasma and demonstrates a high recovery of 100% for low concentration of 1 pM. The aptasensor could be generalized to various proteins detection involving specific aptamers.

Acknowledgments

This work was supported by France Government and the Slovak Research and Development Agency (Contracts nos. APVV-0410-10 and SK-FR-0025-09) and VEGA (Project no. 1/0785/12). We are grateful to Dr. Human Rezaei and Dr. Jasmina Vidic from VIM group of INRA France for generous gift of PrP^C proteins.

References

Bibby, D.F., Gill, A.C., Kirby, L., Farquhar, C.F., Bruce, M.E., Garson, J.A., 2008. J. Virol. Methods 151, 107–115.
Bard, A.J., Faulkner, L.R., 2001. Electrochemical Methods: Fundamentals and Applications, second ed. Wiley, New York.
Chen, W., Li, C.M., Chen, P., Sun, C.Q., 2006. Electrochim. Acta 52, 2845–2849.
Chebil, S., Hafaiedh, I., Sauriat-Dorizon, H., Jaffrezic-Renault, N., Errachid, A., Ali, Z., Korri-Youssoufi, H., 2010. Biosens. Bioelectron. 26, 736–742.
Collinge, J., 2001. Annu. Rev. Neurosci. 24, 519–550.
Fournier-Wirth, C., Jaffrezic-Renault, N., Coste, J., 2010. Transfusion 50, 2032–2045.
Grosjean, L., Cherif, B., Mercey, E., Roget, A., Levy, Y., Noel Marche, P., Villiers, M.-B., Livache, T., 2005. Anal. Biochem. 347, 193–200.
Ho, H.A., Doré, K., Boissinot, M., Bergeron, M.G., Tanguay, R.M., Boudreau, D., Leclerc, M., 2005. J. Am. Chem. Soc. 127, 12673–12676.
Ingrosso, L., Vetrugno, V., Cardone, F., Pocchiari, M., 2002. Trends Mol. Med. 8, 273–280.
Kawatake, S., Nishimura, Y., Sakaguchi, S., Iwaki, T., Dohura, K., 2006. Biol. Pharm. Bull. 29, 927–932.
Korri-Youssoufi, H., Garnier, F., Srivastava, P., Godillot, P., Yassar, A., 1997. J. Am. Chem. Soc. 119, 7388–7389.
Korri-Youssoufi, H., Makrouf, B., 2001. Synth. Met. 119, 265–266.
Korri-Youssoufi, H., Yassar, A., 2001. Biomacromolecules 2, 58–64.
Kuczius, T., Koch, R., Keyvani, K., Karch, H., Grassi, J., Groschup, M.H., 2007. Eur. J. Neurosci. 25, 2649–2655.
Laviron, E.J., 1979. Electroanal. Chem. 101, 19–28.
Lê, H.Q.A., Sauriat-Dorizon, H., Korri-Youssoufi, H., 2010a. Anal. Chim. Acta 674, 1–8.
Lê, H.Q.A., Chebil, S., Makrouf, B., Sauriat-Dorizon, H., Mandrand, B., Korri-Youssoufi, H., 2010b. Talanta 81, 1250–1257.
Liu, G., Liu, J., Böcking, T., Eggers, P.K., Gooding, J., 2005. Chem. Phys. 319, 136–146.
Livache, T., Bazin, H., Mathias, G., 1998. Clin. Chim. Acta 278, 171–176.
Masters, C.L., Gajdusek, D.C., Gibbs Jr., C.J., 1981. Brain 104, 559–588.
Miodek, A., Poturnayová, A., Snejdárková, M., Hianik, T., Korri-Youssoufi, H., 2013a. Anal. Bioanal. Chem. 405, 2505–2514.
Miodek, A., Castillo, G., Hianik, T., Korri-Youssoufi, H., 2013b. Anal. Chem. 85, 7704–7712.
Nkosi, D., Pillay, J., Ozemena, K., Nouneth, K., Oyama, M., 2010. Chem. Phys. Chem. Phys. 12, 604–613.
Nunnally, B.K., 2002. Trends Anal. Chem. 21, 82–89.
Pan, K.M., Baldwin, M., Nguyen, J., Gasset, M.D., Serban, A., Groth, D., Mehlhorn, I., Huang, Z., Fletterick, J., Cohen, F.E., Prusiner, S.B., 1993. Proc. Natl. Acad. Sci. USA 90, 10962–10966.
Panigaj, M., Brouckova, A., Glierova, H., Dvorakova, E., Simak, J., Vostal, J.G., Holada, K., 2011. Transfusion 51, 1012–1021.
Prusiner, S.B., 1991. Science 252, 1515–1522.
Prusiner, S.B., Scott, M.R., DeArmond, S.J., Cohen, F.E., 1998. Cell 93, 337–348.
Ramanavičius, A., Ramanavičiene, A., Malinauskas, A., 2006. Electrochim. Acta 51, 6025–6037.
Safar, J.G., Geschwind, M.D., Deering, C., Didorenko, S., Sattavat, M., Sanchez, H., Serban, A., Vey, M., Baron, H., Giles, K., Miller, B.L., Dearmond, S.J., Prusiner, S.B., 2005. Proc. Natl. Acad. Sci. USA 102, 3501–3506.
Şenel, M., Nergiz, C., 2012. Synth. Met. 162, 688–694.
Şenel, M., Çevik, E., 2012. Curr. Appl. Phys. 12, 1158–1165.
Takemura, K., Wang, P., Worberg, I., Surewicz, W., Priola, S.A., Kanthasamy, A., Pottathil, R., Chen, S.G., Sreevatsan, S., 2006. Exp. Biol. Med. 231, 204–214.
Tlili, C., Korri-Youssoufi, H., Ponsonnet, L., Martelet, C., Jaffrezic-Renault, N., 2005. Talanta 68, 131–137.
Tsukruk, V.V., Rinderspacher, F., Bliznyuk, V.N., 1997. Langmuir 13, 2171–2176.
Shi, W.-J., Ai, S.-Y., Li, J-H., Zhu, L.-S., 2008. Chin. J. Anal. Chem. 36, 335–338.
Zhu, N., Gao, H., Xu, Q., Lin, Y., Su, L., Mao, L., 2010. Biosens. Bioelectron. 25, 1498–1503.